ELSEVIER

Electrochimica Acta 51 (2006) 1752–1760

Acta

www.elsevier.com/locate/electacta

Characterisation by EIS of ternary Mg alloys synthesised by mechanical alloying

Christopher M.A. Brett [a,*,1], Lidia Dias [b], Bruno Trindade [b], Robert Fischer [a], Sascha Mies [a]

[a] *Departamento de Quimica, Universidade de Coimbra, 3004-535 Coimbra, Portugal*
[b] *Departamento de Engenharia Mecânica, Universidade de Coimbra, 3030-201 Coimbra, Portugal*

Received 6 August 2004; received in revised form 17 November 2004; accepted 9 February 2005
Available online 6 September 2005

Abstract

Electrochemical impedance spectroscopy has been used to study the electrochemical behaviour of ternary $Mg_{60}Ti_{10}Si_{30}$ and $Mg_{88}Ti_5Si_7$ alloy samples fabricated by mechanical alloying of the elemental powders in an argon atmosphere. The influence of different milling times up to 25 h and heat treatment on the electrochemical behaviour of the samples, after compacting under pressure into disks, has been investigated in 0.1 M Na_2SO_4 and 0.01 M NaCl electrolyte solutions. Complementary measurements of open circuit potential, polarisation curves, and surface and microstructural analysis have been carried out. The experimental results revealed that corrosion is greater for $Mg_{88}Ti_5Si_7$ which contains free magnesium; however, in sulphate solution a protective oxide layer formed can reduce the corrosion rate. In $Mg_{60}Ti_{10}Si_{30}$, heat treatment increases corrosion, which is explained through a greater tendency for pitting corrosion. Comparison is made between the electrochemical impedance data and the nanophase structure as well as with the electrochemical behaviour of other magnesium alloys.

Keywords: Magnesium alloys; Mechanical alloying; Corrosion; Electrochemical impedance

1. Introduction

Magnesium's low density has led to its being investigated as a major alloy element for use in light-weight components in the automotive and aerospace industries, thus increasing functionality per unit weight. Various types of magnesium alloy have been considered. Most of them have included aluminium with the addition of a third element such as zinc. Different synthesis methods have also been suggested, with a view to controlling the microstructure and in this way improving the properties. The limiting factor in nearly all cases is the poor corrosion resistance of the alloys, owing to the high activity of magnesium, particularly in a saltwater environment [1], and thus alloying elements have been chosen particularly with a view to its improvement. Candidates for this purpose include aluminium, referred to above, and titanium, both of which form a self-healing corrosion layer, although this is much more effective in the case of titanium [2]. Titanium's mechanical properties are also superior to those of aluminium. Unfortunately, magnesium and titanium are almost mutually insoluble and so normal alloying mixing processes are not feasible. Only far-from-equilibrium processes such as mechanical alloying (MA) and physical vapour deposition (PVD) techniques can be successfully employed. A third element with a great affinity for titanium and magnesium can be also incorporated in order to increase alloy strength by formation of fine-dispersion precipitates of intermetallic phases in the Mg matrix, the resulting alloys being designated as metal matrix composite (MMC) materials. This can be achieved by addition of silicon, since it forms intermetallic compounds with both Mg and Ti. Mechanical alloying, in which the elements in powder form are mechanically mixed for a chosen period of time, usually under an inert gas atmosphere to avoid oxidation or contamination, has been

* Corresponding author. Tel.: +351 239 835295; fax: +351 239 835295.
E-mail address: brett@ci.uc.pt (C.M.A. Brett).
[1] ISE member.

0013-4686/$ – see front matter © 2005 Elsevier Ltd. All rights reserved.
doi:10.1016/j.electacta.2005.02.124

used for magnesium alloy synthesis [3,4], and in particular for the MgTiSi system [5–7].

Magnesium has been the object of a number of electrochemical and corrosion studies in chloride and sulphate solutions [8–12], mainly with a view to a greater understanding of the behaviour of its alloys. Although the effect of the aggressive chloride ion is of paramount importance, many studies use sulphate ion in order to study the corrosion processes occurring. The effect of pH and pH buffering has also been investigated since the rate of corrosion diminishes significantly in alkaline solution.

Several magnesium alloys have also been studied [12–19], particularly AZ91, which is a dual phase magnesium–aluminium–zinc alloy. Various electrochemical techniques, including electrochemical impedance spectroscopy, together with surface analysis, have been used to probe the mechanism of corrosion and the effect of alloy microstructure. Types of corrosion observed include pitting, filiform and granular corrosion. The influence of testing parameters on the corrosion rate has been investigated [20], as has the nanocrystallinity [21] and the increase of corrosion resistance by coating with electroless nickel after chemical conversion of the surface [22]. Other studies have addressed the problem of galvanic corrosion [23] and of atmospheric corrosion-temperature, relative humidity and chloride deposition [24].

Present understanding of the mechanism of corrosion of magnesium alloys has been reviewed in the light of their use in the transportation industry [25,26], complicated by the negative difference effect, i.e. the increase in both anodic and cathodic reactions as the potential increases above the open circuit value, and by fatigue-induced corrosion [27].

To our knowledge, the electrochemical behaviour of magnesium alloys prepared by mechanical alloying has been little investigated. Ozaki et al. studied the corrosion behaviour of bulk amorphous $Mg_{75}Ni_{15}Si_{10}$ alloy [28]. Grosjean et al. investigated the effect of ball milling on the corrosion resistance of pure magnesium in alkaline aqueous media, finding an improvement which they attributed to increased surface defects and grain boundaries where a protective magnesium hydroxide layer could be formed [29].

This paper deals with the influence of the nanostructure on the corrosion behaviour of mechanically alloyed $Mg_{60}Ti_{10}Si_{30}$ and $Mg_{88}Ti_5Si_7$ samples with and without annealing, studied by electrochemical impedance spectroscopy (EIS). The as-mechanically alloyed powders have been previously characterised by X-ray diffraction and scanning electron microscopy and their thermal stability evaluated by differential scanning calorimetry (DSC) [30].

2. Experimental

2.1. Sample preparation

Samples of nominal compositions (wt.%) $Mg_{60}Ti_{10}Si_{30}$ and $Mg_{88}Ti_5Si_7$ were synthesised by mechanical alloying from Mg, Si and Ti powders with purity of 99.6%, 99.5% and 99.0% and average particle sizes of 60, 10 and 75 μm, respectively. Milling was performed in a Fritsch Pulverisette 6 planetary ball mill using a hardened steel vial (250 ml) and balls (15 balls of 20 mm diameter each) for times between 1 and 25 h. The ball-to-powder weight ratio was 20:1, and the rotation speed was 500 rpm. In order to avoid contamination, milling was performed in an argon atmosphere.

2.2. Structural analysis of samples

The powder samples obtained by milling were analysed by X-ray diffraction (XRD) with Co Kα radiation and scanning electron microscopy (SEM). Based on the DSC curves [30], the milled samples were annealed in a vacuum furnace at 500 and 900 °C ($Mg_{60}Ti_{10}Si_{30}$ samples) or at 300 and 500 °C ($Mg_{88}Ti_5Si_7$ samples). The structure of the mixtures was evaluated at room temperature by XRD.

2.3. Electrochemical experiments

For electrochemical experiments, the powders were compacted with a uniaxial pressure of 470 MPa into 10 mm diameter disks of 1 mm thickness; there was no visible porosity by microscopy. They were mounted as electrodes, by attaching a wire onto one face using silver epoxy and then covering this and the rest of the sample with normal epoxy resin, except for one disc surface. Immediately before experiments the surface was mechanically polished with SiC abrasive paper down to 1800 grit and rinsed with acetone.

Electrochemical experiments were carried out in 0.01 M NaCl and 0.1 M Na_2SO_4 aqueous solutions, chosen in order to permit comparisons with results in the literature for other magnesium alloys. All solutions were made with analytical grade chemical reagents and Millipore Milli-Q water (resistivity > 18 MΩ cm). Experiments were carried out at room temperature (25 ± 1 °C). The electrochemical cell also contained a platinum foil auxiliary electrode and a saturated calomel electrode (SCE) as reference.

Measurements of the open circuit potential (OCP) and its variation with time, and the recording of polarisation curves were done using a Princeton Applied Research PAR 273A potentiostat. Electrochemical impedance spectra were recorded at an applied potential equal to the open circuit potential at the beginning of the experiment, after immersion in electrolyte solution for enough time in order to attain a sufficiently constant value of the OCP—2.5 h for $Mg_{60}Ti_{10}Si_{30}$ and 1 h for $Mg_{88}Ti_5Si_7$. A Solartron 1250 Frequency Response Analyser coupled to a 1286 Electrochemical Interface controlled by ZPlot software was employed over the frequency range 10 kHz to 0.1 Hz, or lower down to a minimum of 1 mHz if the system was sufficiently stable over the experimental timescale, which only occurred in sodium sulphate solution after heat treatment with $Mg_{60}Ti_{10}Si_{30}$ samples. A 10 mV rms sinusoidal voltage perturbation was used and five steps per frequency decade.

3. Results and discussion

3.1. Structural analysis of the milled samples with and without subsequent heat treatment

Characterisation of the alloys by XRD clearly showed the structural order of the magnesium phase decreasing with milling time [30]. The intermetallic Mg_2Si is formed already at the beginning of the process. For the lower silicon content sample the final structure after milling is Mg_2Si in a Mg matrix; for the other, Ti_5Si_3 is formed with the remaining silicon not used in the formation of Mg_2Si (Fig. 1a). Very little structural change occurred during heat treatment of the samples, see Fig. 1b.

XRD analysis did not show any phase transformation of the $Mg_{60}Ti_{10}Si_{30}$ sample up to 500 °C. However, annealing at higher temperatures (900 °C) gave rise to another intermetallic ($TiSi_2$), which might be the result of partial decomposition of Mg_2Si followed by the reaction of Ti_5Si_3 with Si to form $TiSi_2$ and Mg with residual oxygen from the environment to form MgO phases (Fig. 1b). An increase of the grain size of the Mg_2Si and Ti_5Si_3 phases is also observed during heat treatment (Table 1). Concerning the $Mg_{88}Ti_{10}Si_7$Tsample, the only noticeable feature is the increase of the XRD peak intensity and the decrease of the peak width at half height meaning growth in grain size of the Mg and Mg_2Si phases. In spite of this growth, both samples are nanocrystalline even after heat treatment.

3.2. Influence of immersion time on open circuit potential and corrosion rate

Open circuit potential experiments were conducted in 0.01 M NaCl and 0.1 M Na_2SO_4 solutions. Typical examples of traces obtained in 0.01 M NaCl electrolyte for the two types of sample after 25 h milling are shown in Fig. 2. For both types of sample in 0.1 M Na_2SO_4, and for the $Mg_{60}Ti_{10}Si_{30}$ in 0.01 M NaCl, the variation of open circuit potential was of the form of that in Fig. 2a, reaching a relatively constant value after less than 1 h immersion. There was also the formation of a black layer on the sample surface, attributed to the formation of oxides (see below) and pitting corrosion then began to occur. For $Mg_{88}Ti_5Si_7$ in 0.01 M NaCl, which contains free magnesium, the potential increased rapidly over a period of 1 min and then became slightly more negative before becoming more positive again and reaching a steady value—this type of behaviour occurred for samples milled for different times and with our without heat treatment. The initial sharp variation is due to magnesium corrosion, then there is some

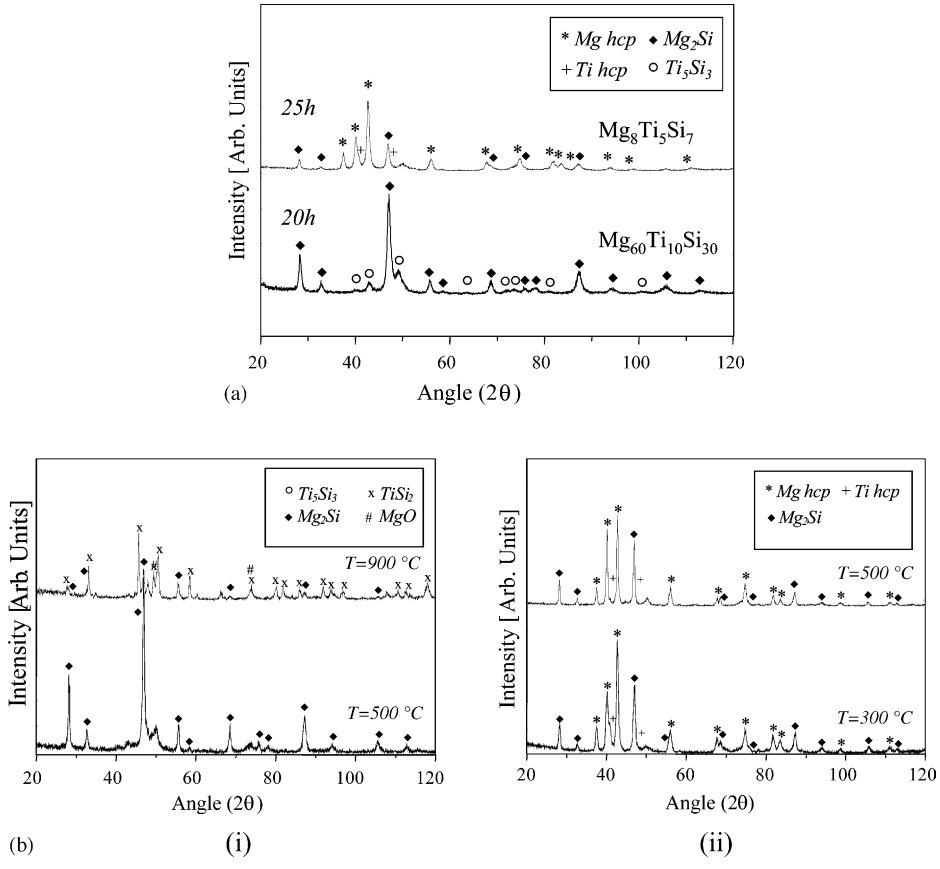

Fig. 1. XRD patterns of samples of: (a) mechanically alloyed $Mg_{60}Ti_{10}Si_{30}$ and $Mg_{88}Ti_5Si_7$; (b) heat-treated (i) $Mg_{60}Ti_{10}Si_{30}$ and (ii) $Mg_{88}Ti_5Si_7$.

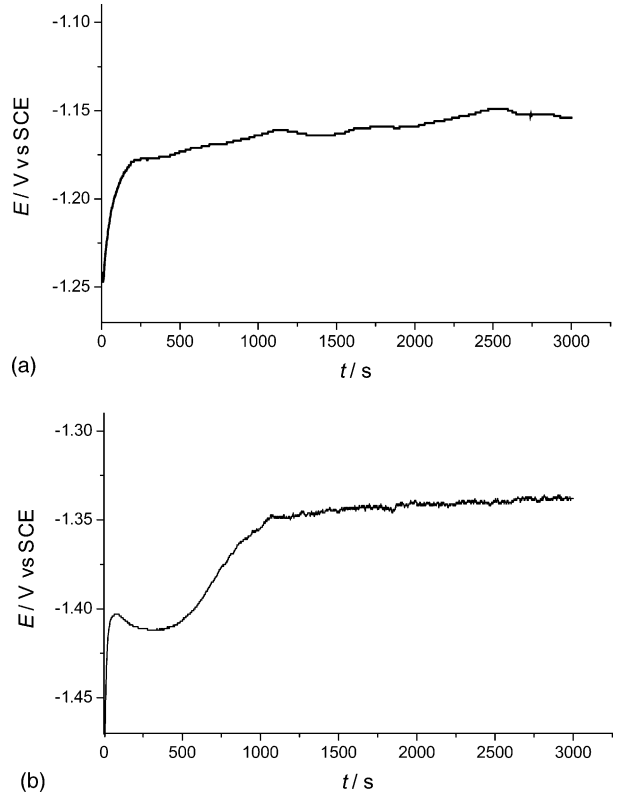

Fig. 2. Variation with time of open circuit potential following immersion in 0.01 M NaCl solution of (a) $Mg_{60}Ti_{10}Si_{30}$ and (b) $Mg_{88}Ti_5Si_7$ samples after 25 h milling.

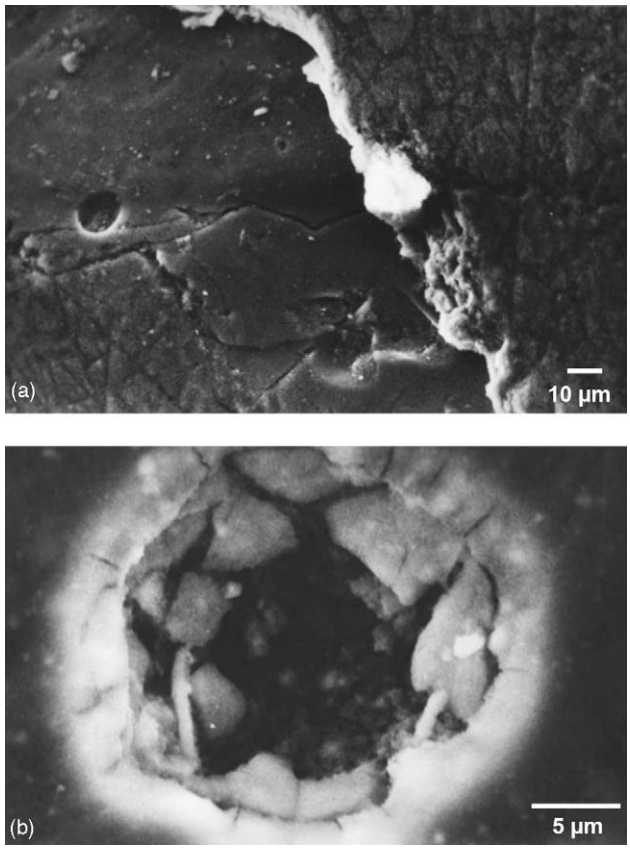

Fig. 3. Scanning electron microscopy of corroded areas of (a) $Mg_{60}Ti_{10}Si_{30}$ and (b) $Mg_{88}Ti_5Si_7$ samples after immersion in 0.1 M Na_2SO_4 solution for 3 h.

protective oxide formation. Since the samples have a small porosity as well as phase boundaries, the effect of electrolyte penetration probably caused the further smaller shift in the positive direction.

The surfaces of the samples were examined by scanning electron microscopy following corrosion and showed the formation of tiny pits and flaws, even in the less aggressive 0.1 M Na_2SO_4 solution, shown in Fig. 3, and much more evident for the $Mg_{88}Ti_5Si_7$ sample, see example in Fig. 3b. Chemical microanalysis confirmed the formation of a layer of titanium and magnesium oxides in all cases.

Polarisation curve analysis [30] did not permit clear distinctions between the different milling times and heat treatments in sodium sulphate solution, with corrosion currents of the order of 10–40 $\mu A\,cm^{-2}$. However, in sodium chloride solution currents could reach an order of magnitude higher and differences became apparent between the various sintering conditions and heat treatments for the alloys. This is illustrated in the curves of Fig. 4, where the differences in corrosion potential and corrosion current are clearly evident. General conclusions from these tests were that for the $Mg_{60}Ti_{10}Si_{30}$ sample, which shows a much lower corrosion current, increased milling time and heat treatment does not significantly change the corrosion current values, whereas for the $Mg_{88}Ti_5Si_7$ sample, increased milling and heat treatment up to 300 °C both reduce the corrosion current, which increases again following heat treatment at 500 °C. This suggests that the nanostructure plays a significant role and will be discussed further below.

The information from open circuit potential and polarisation experiments was used for choosing the best conditions and immersion time for carrying out the electrochemical impedance experiments.

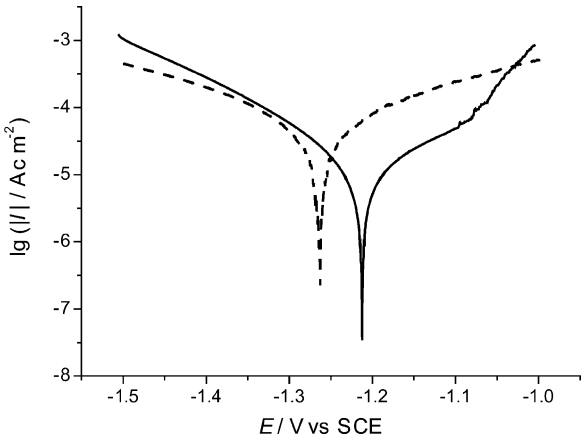

Fig. 4. Polarisation curves for a $Mg_{88}Ti_5Si_7$ sample after heat treatment at 300 °C immersed in (—) 0.1 M Na_2SO_4 and (- - -) 0.01 M NaCl.

3.3. Electrochemical impedance

Representative complex plane spectra are shown in Figs. 5–8 for the two types of sample in the two electrolyte solutions tested and for different conditions of milling time and heat treatment. The electrochemical impedance spectra showed some variation from one sample to another, which reflects the variations in composition of the sintered samples. For this reason, the experiments were repeated several times in all cases.

Examination of the spectra reveals significant differences between the two electrolyte solutions in the case of $Mg_{60}Ti_{10}Si_{30}$ samples, Figs. 5 and 6. It should be remembered that in this case there is, in principle, no free magnesium in the matrix. According to the compositional analysis of the materials, after 10 h milling a small amount of Mg has not yet been transformed into Mg_2Si, which can explain differences between the spectra after 10 and 25 h milling in both sulphate and chloride solution. The increase of the grain size of phases Mg_2Si and Ti_5Si_3 after 500 °C heat treatment, Table 1, is reflected in the altered impedance spectra. Heat treatment at 900 °C causes structural changes with formation of $TiSi_2$ (and a tiny amount of MgO) and the spectra change significantly. The low-frequency inductive loop appearing in NaCl solution after 900 °C heat treatment can be ascribed to chloride-induced pit formation. A final point to note is that the potential is sufficiently stable after heat treatment in both sodium sulphate and sodium chloride electrolytes to permit reaching frequencies lower than 0.01 Hz (5 min data acquisition time). The correlation of these changes and the impedance spectra will be discussed further in the following section.

Table 1
Grain size of the $Mg_{60}Ti_{10}Si_{30}$ and $Mg_{88}Ti_5Si_7$ milled samples heat treated at different temperatures

Condition	$Mg_{60}Ti_{10}Si_{30}$			$Mg_{88}Ti_5Si_7$	
	Mg_2Si (nm)	Ti_5Si_3 (nm)	$TiSi_2$ (nm)	Mg (nm)	Mg_2Si (nm)
25 h milling	20	4	–	40	20
T = 300 °C	–	–	–	45	36
T = 500 °C	37	8	–	60	50
T = 900 °C	45	11	32	–	–

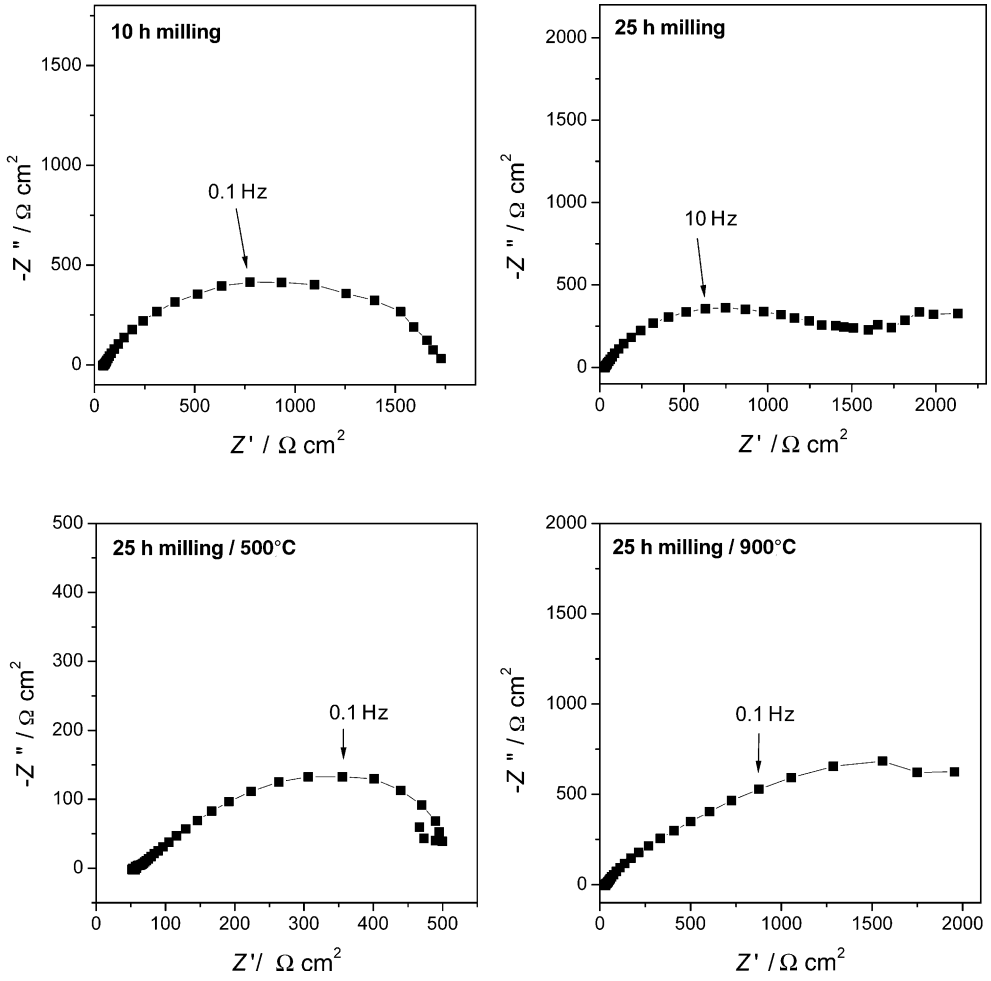

Fig. 5. Representative complex plane impedance spectra, showing the effect of milling time and heat treatment on $Mg_{60}Ti_{10}Si_{30}$ samples recorded in 0.1 M Na_2SO_4 solution after 2.5 h immersion.

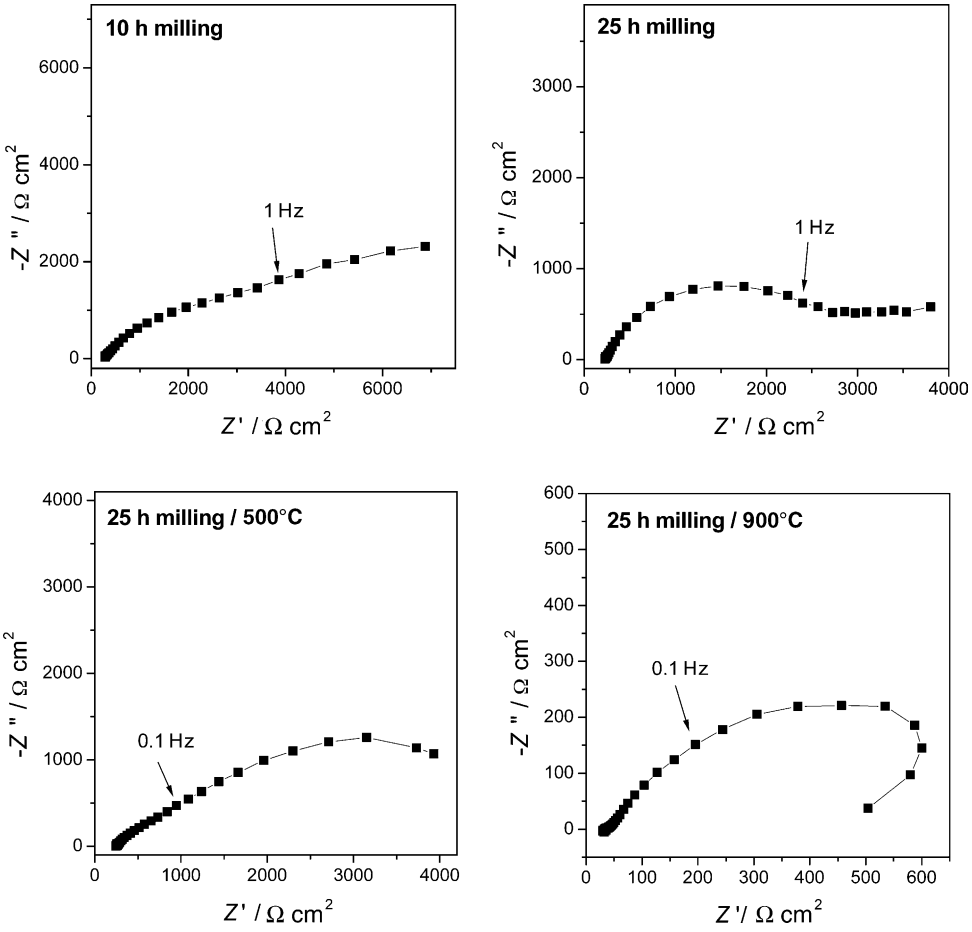

Fig. 6. Representative complex plane impedance spectra, showing the effect of milling time and heat treatment on $Mg_{60}Ti_{10}Si_{30}$ samples recorded in 0.01 M NaCl solution after 2.5 h immersion.

Regarding the $Mg_{88}Ti_5Si_7$ samples, which contain free magnesium, titanium and Mg_2Si after milling, the spectra are much more similar to those of other magnesium alloys, e.g. [16], and the impedance values are, in general, smaller than for the $Mg_{60}Ti_{10}Si_{30}$ samples. Considering the capacitive loop, the time constant remains similar for all milling and heat treatment conditions tested in both electrolyte solutions, contrasting with the changes seen for the other sample type. In sodium sulphate solution there are indications of a low frequency inductive loop which can be attributed to relaxation processes as for other magnesium alloys, as well as in chloride solution, that is probably due to pit formation.

The semi-circular loops at high frequencies in the spectra were modelled using a parallel combination of a resistance, *R*, and a constant phase element (CPE) in series with the cell resistance representing the film and charge transfer effects [11], where the CPE models a non-ideal capacitor. Whilst from inspection of the spectra in Figs. 5–8 it is clear that this can be applied to $Mg_{88}Ti_5Si_7$ samples, for the other sample type the semicircular form is less clear, and the spectra are more complex. Therefore, a sufficiently reasonable frequency range was chosen for fitting the "high frequency" part of the spectra in order to obtain equivalent circuit values for comparative purposes, but it should be noted that the model is clearly a significant simplification of the interfacial processes.

The capacity values, in the $Mg_{60}Ti_{10}Si_{30}$ samples, were of the order of 100–300 $\mu F\,cm^{-2}$ with a roughness exponent between 0.6 and 0.7. In the case of $Mg_{88}Ti_5Si_7$ samples, values were between 100 and 200 $\mu F\,cm^{-2}$ and the roughness exponent was higher at around 0.8. The reason for this can probably be traced to the fact that the latter samples contain magnesium which forms an oxide layer on the surface, thus reducing any effect of localised roughness or structural imperfections and surface flaws.

The values of *R* obtained are given in Table 2, from the average of several spectra. It was difficult to register reproducible spectra for $Mg_{60}Ti_{10}Si_{30}$ in 0.01 M NaCl solution. In the case of $Mg_{60}Ti_{10}Si_{30}$ in 0.1 M Na_2SO_4 solution, which was does not show a clear semicircle, fitting was done down to a frequency of 1 Hz. Table 2 shows that heat treatment appears not to be beneficial for the corrosion resistance. By contrast, in the $Mg_{88}Ti_5Si_7$ samples, where there is free magnesium, the values increase in sulphate solution, but in chloride electrolyte the benefits arising from long milling times are removed on heat treatment, when the Mg_2Si grain size increases, apparently leading to easier attack.

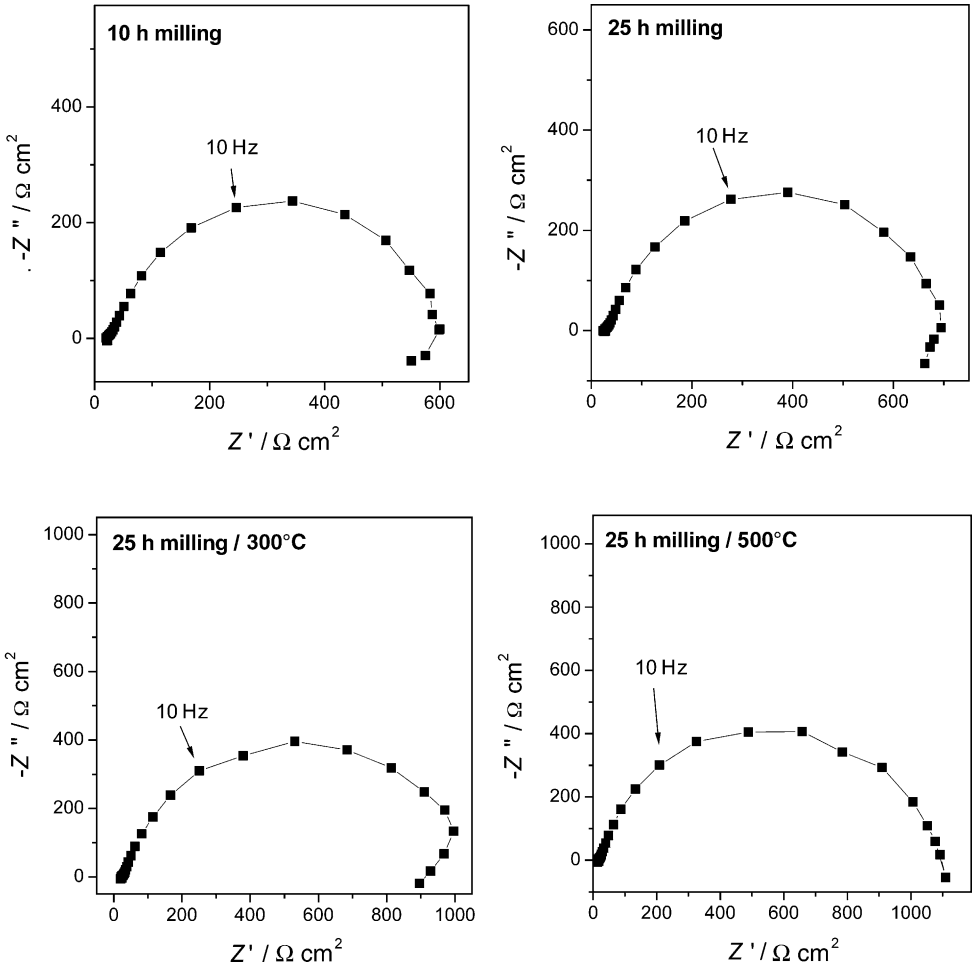

Fig. 7. Representative complex plane impedance spectra, showing the effect of milling time and heat treatment on $Mg_{88}Ti_5Si_7$ samples recorded in 0.1 M Na_2SO_4 solution after 1 h immersion.

3.4. Discussion and comparison with other Mg alloys

The nanostructure of the alloys can aid in explaining the electrochemical results and the EIS results throw further light on the corrosion process, in ways which are not possible with other techniques.

Table 2
Average values of polarisation resistance, *R*, for the mechanically alloyed samples from impedance spectra after immersion in electrolyte for 1 h ($Mg_{60}Ti_{10}Si_{30}$) and 2.5 h ($Mg_{88}Ti_5Si_7$)

	R (Ω cm^2)	
	0.1 M Na_2SO_4	0.01 M NaCl
$Mg_{60}Ti_{10}Si_{30}$		
10 h milling	2000	–
25 h milling	1600	2500
25 h milling/500 °C	500	–
25 h milling/900 °C	800	600
$Mg_{88}Ti_5Si_7$		
10 h milling	610	210
25 h milling	680	420
25 h milling/300 °C	1000	220
25 h milling/500 °C	1020	100

Both types of sample contain Mg_2Si phases of different grain size, varying from 20 nm after milling to 45–60 nm after heat treatment, see Table 1, and which have been suggested to be good pit initiation sites [11]. Regarding $Mg_{60}Ti_{10}Si_{30}$, the increase in Mg_2Si grain size on heat treatment would therefore increase the corrosion rate, which is in agreement with the *R* values obtained from the impedance spectra, Table 2. The component Ti_5Si_3 appears to exert less influence; the lower corrosion rate at 900 °C is probably due to the reduced length of exposed interphase boundaries rather than the appearance of $TiSi_2$.

The behaviour of $Mg_{88}Ti_5Si_7$ is dominated by the free magnesium and Mg_2Si plays a secondary role. Thus, it is easier for the protective oxide film formed in solution on the magnesium to cover the whole surface, as occurs in sulphate solution; increasing grain size enhances this tendency. In sodium chloride solution, however, the formation of small pits in the surface, discussed earlier, has a greater influence together with the possibility of Mg_2Si nucleation sites – these phases also increase in size – and the opposite trend is seen with increase rate of corrosion and lower polarisation resistance.

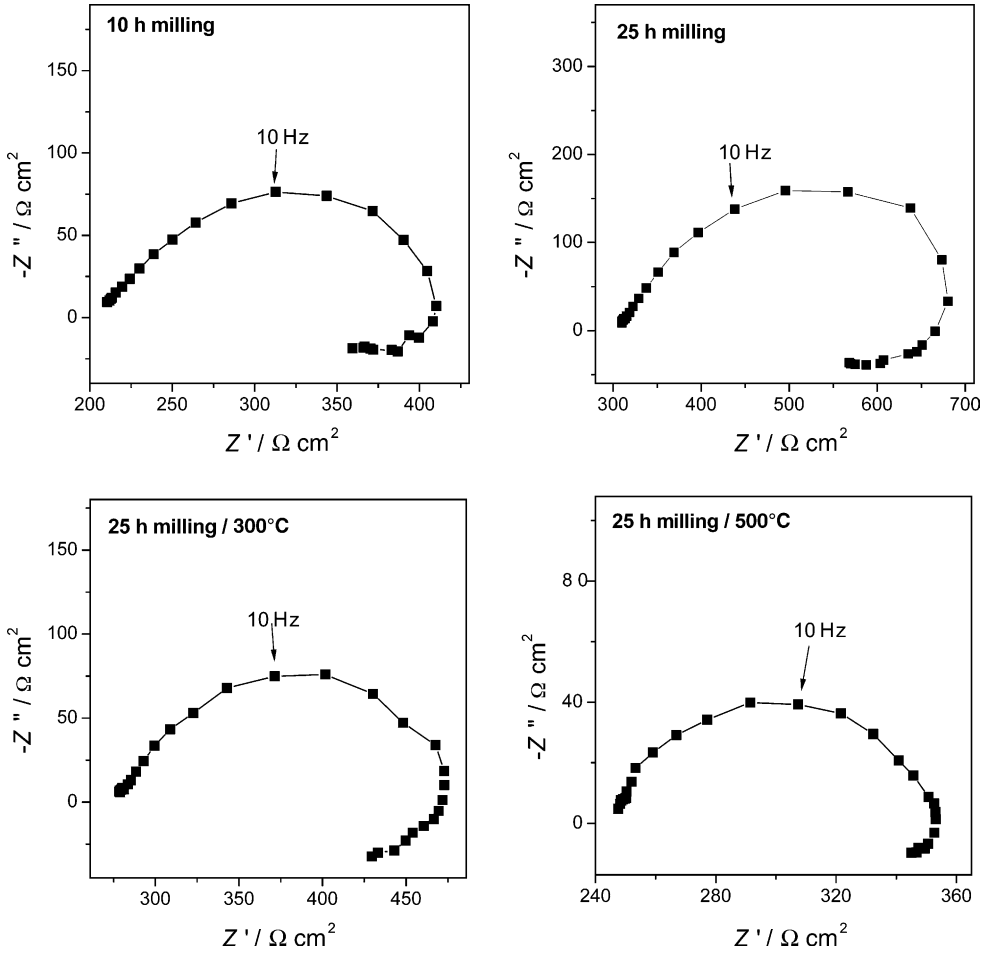

Fig. 8. Representative complex plane impedance spectra, showing the effect of milling time and heat treatment on $Mg_{88}Ti_5Si_7$ samples recorded in 0.01 M NaCl solution after 1 h immersion.

It is instructive to compare the EIS results obtained with those of AZ91 alloy and AZ91 alloy with a higher silicon content [15,16]. These alloys contain, besides magnesium, aluminium, manganese and zinc and a small percentage of silicon which gives rise to Mg_2Si [15]. In these cases, normally three loops appear in the impedance spectra, two capacitive loops and an inductive loop. The high frequency capacitive loop has been ascribed to charge transfer and the film of corrosion products formed. The medium frequency capacitive loop has been attributed to the relaxation of mass transport in the solid phase and disappears at long immersion time [15]. In the present study, a medium frequency capacitive loop appears for $Mg_{60}Ti_{10}Si_{30}$, but is not clearly separated from the high frequency loop—however, the phase nanostructure is completely different. Finally, the inductive loop at low frequency is due to the relaxation of adsorbed species such as $Mg(OH)_{ads}^{+}$ or $Mg(OH)_2$. The low frequency inductive loop is evident in the $Mg_{88}Ti_5Si_7$ samples where there is free magnesium, as in the AZ91 alloy.

Although EIS experiments were carried out at the open circuit potential, some consideration should be given to the negative difference effect, owing to its pernicious effects on the corrosion of pure magnesium and magnesium alloys. This is because a potential positive of the open circuit potential oxidation of magnesium gives rise to Mg^{+} which is then hydrolysed leading to hydrogen evolution and $Mg(OH)_2$. This is a further reason, besides the higher corrosion resistance, to use the $Mg_{60}Ti_{10}Si_{30}$ alloy.

4. Conclusions

Electrochemical impedance has been used to characterise magnesium-titanium-silicon ternary alloys produced by mechanical alloying. It has been shown to be extremely useful, allied with other electrochemical techniques, for the evaluation of the corrosion resistance of these systems, furnishing extra, valuable information for the characterisation of the corrosion process. EIS shows the diagnostic features of the alloys, demonstrates clearly the influence of milling time and heat treatment and brings out better than other techniques the problems of sample surface reproducibility which is one of the most crucial factors for examining and predicting the performance of these types of alloy under service conditions.

It was shown that the corrosion resistance of the $Mg_{60}Ti_{10}Si_{30}$ alloy is higher than that of $Mg_{88}Ti_5Si_7$, owing to its chemical composition and changes in the alloy microstructure occurred during milling and subsequent heat treatment, the latter reducing the corrosion resistance. For the $Mg_{88}Ti_5Si_7$ alloy, the corrosion resistance increases with milling time and the influence of heat treatment depends on the bathing electrolyte, and has an impedance behaviour similar to AZ91 magnesium alloys at long immersion times.

Acknowledgement

Financial support from Fundação para a Ciência e a Tecnologia (FCT), ICEMS (Research Unit 103), Portugal, is gratefully acknowledged.

References

[1] D.L. Hawke, J.E. Hillis, M. Pekguleryuz, I. Nkatsugawa, in: M.M. Avedesian, H. Baker (Eds.), Magnesium and Magnesium Alloys, ASM International, Materials Park, 1999, p. 194.
[2] S.B. Dodd, S. Morris, M. Wardclose, in: F.H. Froes (Ed.), Synthesis of Lightweight Metals III, Minerals Metals and Materials Society, Warrendale, 1999, p. 117.
[3] T. Aizawa, Mater. Sci. Forum 350–351 (2000) 299.
[4] K. Kondoh, E. Yuasa, T. Aizawa, Mater. Sci. Forum 419 (2003) 745.
[5] M. Cavusoglu, O.N. Senkov, F.H. Froes, Key Eng. Mater. 188 (2000) 1.
[6] L. Dias, B. Trindade, C. Coelho, F.H. Froes, Key Eng. Mater. 230–232 (2002) 283.
[7] L. Dias, B. Trindade, C. Coelho, S. Patankar, C. Draney, F.H.S. Froes, Mater. Sci. Eng. A 364 (2004) 273.
[8] N. Pébère, C. Riera, F. Dabosi, Electrochim. Acta 35 (1990) 555.
[9] G. Song, A. Atrens, D. St. John, J. Nairn, Y. Li, Corros. Sci. 39 (1997) 855.
[10] G. Song, A. Atrens, D. St. John, X. Wu, J. Nairn, Corros. Sci. 39 (1997) 1981.
[11] G. Baril, N. Pebère, Corros. Sci. 43 (2001) 471.
[12] H. Inoue, K. Sugahara, A. Yamamoto, H. Tsubakin, Corros. Sci. 44 (2002) 603.
[13] G. Song, A. Atrens, X. Wu, B. Zhang, Corros. Sci. 40 (1998) 1769.
[14] E. Ghali, Mater. Sci. Forum 350–351 (2000) 261.
[15] G. Baril, C. Blanc, N. Pébère, J. Electrochem. Soc. 148 (2001) 489.
[16] G. Baril, C. Blanc, M. Keddam, N. Pébère, J. Electrochem. Soc. 150 (2003) 488.
[17] S. Mathieu, C. Rapin, J. Steinmetz, P. Steinmetz, Corros. Sci. 45 (2003) 2741.
[18] E. Ghali, W. Dietzel, K.U. Kainer, J. Mater. Eng. Perf. 13 (2004) 7.
[19] K. Lips, P. Schmutz, M. Heer, P.J. Uggiowitzer, S. Virtanen, Mater. Corros. 55 (2004) 5.
[20] M. Kühlein, U. Galovsky, Mater. Corros. 55 (2004) 444.
[21] E. Sikora, X.J. Wei, B.A. Shaw, Corrosion 60 (2004) 387.
[22] H. Huo, Y. Li, F. Wang, Corros. Sci. 46 (2004) 1467.
[23] G. Song, B. Johannesson, S. Hapugoda, D. St. John, Corros. Sci. 46 (2004) 955.
[24] N. LeBozec, M. Jonsson, D. Thierry, Corrosion 60 (2004) 356.
[25] G. Song, A. Atrens, Adv. Eng. Mater. 1 (1999) 11.
[26] G. Song, A. Atrens, Adv. Eng. Mater. 5 (2003) 837.
[27] C. Potzes, K.U. Kainer, Adv. Eng. Mater. 6 (2004) 281.
[28] K. Ozaki, A. Matsumoto, A. Sugiyama, T. Nishio, K. Kobayashi, Mater. Trans. JIM 41 (2000) 1495.
[29] M.-H. Grosjen, M. Zidoune, L. Roué, J. Huot, R. Schulz, Electrochim. Acta 49 (2004) 2461.
[30] L. Dias, B. Trindade, R. Fischer, S. Mies, C.M.A. Brett, Mater. Sci. Forum 455–456 (2004) 317.